9-2019

Historical Changes in Lower Columbia River and Estuary Floods: A Numerical Study

Lumas Helaire
Portland State University, helaire@pdx.edu

Stefan Talke
Portland State University, talke@pdx.edu

David A. Jay
Portland State University, djay@pdx.edu

Andrew Mahedy
Portland State University

Citation Details

Helaire, L. T., Talke, S. A., Jay, D. A., & Mahedy, D. (2019). Historical Changes in Lower Columbia River and Estuary Floods: A Numerical Study. Journal of Geophysical Research: Oceans, 124.

JGR Oceans

RESEARCH ARTICLE
10.1029/2019JC015055

Historical Changes in Lower Columbia River and Estuary Floods: A Numerical Study

Lumas T. Helaire[1], Stefan A. Talke[1], David A. Jay[1], and Drew Mahedy[1,2]

[1]Civil and Environmental Engineering Department, Portland State University, Portland, OR, USA, [2]Deceased

Key Points:
- Nineteenth-century bathymetry, tide, and river stage records are used to develop a historical numerical model of the Columbia River Estuary
- Results suggest that water levels are less today than historically during most conditions but approximately equal during most floods
- Frictional effects have decreased over time due to channel deepening and loss of floodplain

Supporting Information:
- Supporting Information S1

Correspondence to:
L. T. Helaire,
helaire@pdx.edu

Citation:
Helaire, L. T., Talke, S. A., Jay, D. A., & Mahedy, D. (2019). Historical changes in Lower Columbia River and estuary floods: A numerical study. *Journal of Geophysical Research: Oceans*, *124*. https://doi.org/10.1029/2019JC015055

Received 13 FEB 2019
Accepted 20 AUG 2019
Accepted article online 10 SEP 2019

Abstract Over the past 150 years, the Lower Columbia River Estuary controlling depth has approximately doubled, the majority of historical wetlands and floodplain have been reclaimed, numerous infrastructure projects have altered and confined flow pathways, and significant natural and anthropogenic changes to the discharge hydrograph have occurred. To investigate the effect of these changes on tides, river slope, and flood water levels, we construct and validate numerical models that simulate flow over late nineteenth-century and present-day bathymetry. The models are validated using archival (1853–1877) and modern tide measurements throughout the Lower Columbia River Estuary and river stage measurements from the tidal river (1876–present). Historical flood plain roughness and levee heights are validated iteratively by requiring simulations to match the observed roll off in the river stage rating curve during floods. Measurements and model results show that environmental change has amplified tidal constituents, with peak change about 60 km from the coast. By contrast, increased depth has reduced river slope for low and moderate river discharge. For rarely observed extreme floods of 30×10^3 m^3/s, simulated modern water levels exceed historical in Portland (OR). These observations highlight competing hydrodynamic effects, which are investigated by scaling the St. Venant equations for a simulated 25×10^3-m^3/s flood: While larger modern depth reduces frictional effects and decreases surface slope, reduced floodplain access confines modern flow into channels, increasing velocity, bed stress, and water levels. However, the highly frictional historical floodplain conveyed little flow, limiting the effect of floodplain to storage effects; hence, most simulated historical floods exceed modern levels.

Plain Language Summary In the Columbia River since the late nineteenth century, there have been significant changes to the river channel and adjacent floodplain to facilitate shipping and economic development (i.e., deeper channel, less marshes, and swamps). Along with these topographical changes, there have also been changes to the river's discharge patterns. We use two sets of computers simulations, one with the topography of today and another with late nineteenth-century topography, to evaluate how changes to river topography affect river tides and floods. We construct and verified the models with archival (1853–1901) and modern water level and topography measurements. The study confirms that under normal flow conditions, the increased channel depth and the loss of swamps and marshes have caused an increase in river tides, an increase in river flow velocity, and a drop in the baseline water levels. Despite the drop in baseline water levels, the peak water level during large floods would be the same in the 1870s and today. It was found that higher modern levees confine river flow and are not overtopped, as opposed to lower 1870s levees that were frequently overtopped. The study highlights how modern development has altered the river's flow characteristics.

1. Introduction

Tidal rivers and estuaries all over the United States have been extensively modified for navigation, agriculture, flood protection, and other uses (USACE (United States Army Corp of Engineers), 1915). Similar infrastructure projects have been implemented worldwide and include channel deepening (often doubling or tripling depth), loss of wetlands, streamlining of channels, narrowing of entrances, and construction of pile dikes and other flow modification structures (Sherwood et al., 1990; Wang et al., 2018). These physical changes are often combined with alterations in the river flow hydrograph, which can be caused by land use changes, water resource management, and/or climate change (Cox et al., 2003; Keshtpoor et al., 2015; Passeri et al., 2015; Manning et al., 2011, Naik & Jay, 2011). Altered bathymetry also has consequences for mean water levels (MWLs) and the dynamics of tide waves and other long waves. In the Cape Fear Estuary (NC), channel deepening caused a doubling of tide range and an amplification of storm surge waves (Familkhalili & Talke, 2016). Similarly, Wang et al. (2018), studying the coastal areas of Shanghai, found that future changes in

storm flooding were more influenced by bathymetric changes than relative sea level rise. In the tidal Hudson River, channel deepening since 1930 reduced the effective drag, increasing the magnitude of tides and coastal storm surge observed in the tidal river (Ralston et al., 2019). However, flow management decreased flood magnitudes, and channel deepening also reduced the river slope. Hence, water level in Albany (NY) during the once-in-10-years event is now nearly 3 m lower than in the late nineteenth/early twentieth century, more than compensating for the increased surge amplitude (Ralston et al., 2019).

In this study, we evaluate how tides and flood propagation within the Lower Columbia River Estuary (LCRE) have changed due to ~150 years of anthropogenic changes, including diking, land reclamation, and channel deepening. Approximately 68–70% of the vegetated tidal wetlands and 55% of the forested uplands have been lost in the LCRE since the late 1800s (Marcoe & Pilson, 2017). Moreover, the mouth of the Columbia has been deepened and narrowed, and channels have been significantly dredged and streamlined for navigation purposes (Bottom et al., 2005). Jay et al. (2010) showed that as a result of changes, MWLs at Vancouver (rkm 170) dropped between 0.3 and 1.5 m since 1902, for river flow levels from 2.5–15 $\times 10^3$ m^3/s. These changes were attributed to decreased flow resistance caused by navigational channel dredging, and bed degradation related to dredging, gravel mining, and a reduction in sand supply caused by the reservoir system (Templeton & Jay, 2012) However, Jay et al. (2010) only considered low and moderate flow conditions at one location, and it remains unclear whether a large flood, such as often occurred in the past, would be higher or lower today than it was historically. Indeed, within a more riverine context, it is often argued that channel deepening and narrowing has increased flood risk (e.g., on the Mississippi River; Pinter et al., 2008; Munoz et al., 2018), in contrast with the Ralston et al. (2019) result on the Hudson River.

Since the magnitude of spring freshets on the Columbia River has been curtailed an average of 45% by reservoir management (e.g., Naik & Jay, 2005), the best (and only) way to determine whether large historical floods would produce larger water levels today, were they to recur in the LCRE, is through numerical modeling. Several previous efforts have been made to develop predictive numerical models to capture the effects of long-term changes in the LCRE. Hamilton (1990) used a two-dimensional model in an early attempt to analyze historical changes to salinity intrusion and tides but focused only on the lower 50 km of the estuary and did not attempt to calibrate their model to historical data. To understand the effects of changing morphology near the ocean entrance, Elias et al. (2012) used the Delft3D modeling system to develop a coupled hydrodynamic and wave model for the estuary mouth. They found that near the mouth of the river, sediment transport in the summer month is controlled by density stratification and is net landward. The Center for Coastal Margin Observation and Prediction has developed models for the purpose of monitoring and scientific research (Kärnä et al., 2015; Kärnä & Baptista, 2016; Zhang et al., 2004; Zhang & Baptista, 2008). These studies, focusing on the Columbia River estuary, provide insight into present-day mixing and transport processes but are not meant to provide insights into long-term trends and system trajectory.

The recent recovery of archival tide data from the nineteenth century (Talke & Jay, 2013; Talke & Jay, 2017), along with the digitization of historical bathymetry (Burke, 2010; see also Marcoe & Pilson, 2017), enables the modeling of late nineteenth-century conditions and interpreting system functioning during less anthropogenically altered periods. Our approach, after developing models based on nineteenth and early 21st century bathymetry (hereafter named "historical" and "modern" models) is to first validate against data, which reflects a range of tidal and fluvial forcing. Next, we simulate a historical flood (the 1880 spring freshet) in both models and evaluate spatial changes to water levels and hydrodynamic processes during both mean and extreme conditions. Through statistical analysis, tidal analysis, and scaling of results, we examine how changing bathymetry and friction have affected the transmission of long waves (floods and tides), with implications for habitat inundation and flood risk.

2. Background

2.1. Geography and Hydrology

The Columbia River, with an average discharge of ~7,500 m^3/s, is the largest river on the Pacific Coast of North America and drains an area of 660,480 km^2 (Figure 1; Naik & Jay, 2005). The LCRE, with a length of 230 km, is the tidal river and estuarine section of the Columbia River and stretches from the ocean to Bonneville Dam (Figure 1; Naik & Jay, 2005). The largest tributary, the Willamette

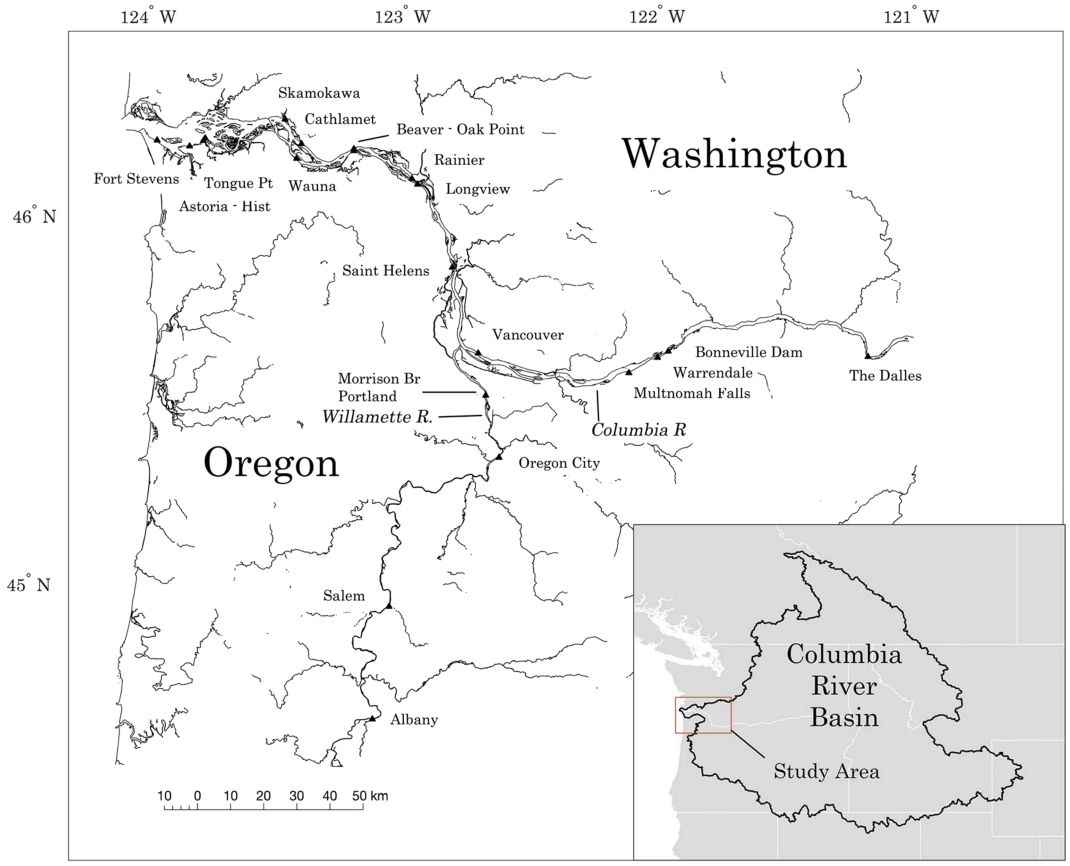

Figure 1. The present-day shoreline of the Lower Columbia River Estuary and gauge stations used in the analysis (triangles).

River, enters the Columbia River at rkm 163, just downstream of Vancouver, WA. Together, the Willamette and the main stem Columbia River provide ~90% of the discharge that flows into the ocean (Orem, 1968). Discharge at The Dalles, Station 14105700, U.S. Geological Survey [USGS]), located ~100 km upstream of Bonneville Dam, accounts for 75% of the flow that reaches the mouth of the river (Naik & Jay, 2011). Several smaller tributaries discharge into the LCRE, including the Cowlitz River, Sandy River, and Lewis River.

Natural and anthropogenic factors have altered river discharge since the 1800s, with the largest factor being the construction of dams along the Columbia River between the 1930s and early 1970s. Combined with a reduction in snowpack due to climate change and the diversion of flow for agriculture, the magnitude of the May/June spring freshets (the primary source of historical floods) has been reduced by 45%; by contrast, the base flow during the July–October low flow periods has increased (Bottom et al., 2005; Naik & Jay, 2011). Consequently, spring freshets between 1850 and 1970 were much larger than the freshets that have occurred since the completion of the reservoir system in the early 1970s.

Tidal statistics and tide range in the LCRE also appear to be changing over secular (century) time scales. Jay (2009) noted a 77-mm-per-century increase in the M_2 constituent and a 35-mm-per-century increase in the K_1 constituent at Astoria since 1925, and Jay et al. (2010) noted an increase in tide range at Vancouver of 0.4 m during low flow conditions. At present, the M_2 amplitude is 0.95 m at Tongue Point (rkm 25; Station 9439040, National Oceanic and Atmospheric Administration [NOAA]), and the K_1 amplitude is 0.4 m (Figure 1). The large K_1/M_2 ratio produces mixed semidiurnal tides, with a large diurnal inequality. In the Portland area, upstream discharge significantly influences tidal range. Under low flow conditions, Vancouver (see Figure 1; Station 9440083, NOAA) exhibits a tidal range as large as 1 m. At high discharge ($>15 \times 10^3$ m^3/s), the tidal signal largely disappears.

2.2. Flood History and Changing Water Levels

During the nineteenth and early twentieth century, communities along the LCRE (Figure 1) were subject to multiple flooding events each decade, with the largest (the 1894 spring freshet) causing the city of Portland to be flooded for approximately 3 weeks. Earlier floods, especially the 1876 and 1880 spring freshets, inundated smaller areas for a longer time. While a combination of flood control reservoirs and levees have reduced flood frequency, river discharge still occasionally exceeds the modern bankfull flow of ~24 × 10^3 m^3/s. Since 1900, there have been five events exceeding this threshold: in 1913 (spring), 1948 (spring), 1956 (spring), 1965 (winter), and 1996 (winter; Waananen et al., 1970; USACE, 1997). Large spring flow peaks in 1956, 1972, 1974 (with probably the largest twentieth century snowpack), 1997, and 2011 were successfully attenuated by reservoir management; however, none of these years combined a very large spring freshet with high spring rainfall, comparable to 1948. Despite the extensive Columbia Basin reservoir system, the combination of a heavy winter snowpack and unexpected spring rains remains a potential system failure mode that can result in dangerous floods, potentially as large or larger than 1948 (Mote & Salathé, 2010; Salathé et al., 2014). This potential for property damage and loss of life underscores the need to understand the response of the system to changes in bathymetry.

2.3. Navigation History

Since 1878, an ongoing effort has been made to maintain a suitable navigation channel, through a series of modifications to the river mouth and channel (Act to Improve Rivers and Harbors, 1878; Public Acts of the 47th Congress, 1882; Rivers and Harbors Appropriation Act, 1899; River and Harbor Act, 1905; River and Harbor Act, 1912; River and Harbor Act, 1930; River and Harbor Act, 1954; Rivers and Harbors Act, 1962; Water Resources Development Act, 1999). These modifications include the construction of jetties near the mouth of the river, dredging of the navigation channel, and the installation of >200 pile dikes by the USACE to encourage scouring and to direct the river along a desired path (Dodge, 1976; Hickson, 1961; Kassenbaum, 2011; Lockett, 1959). The controlling depth of the shipping channel has increased from about 6 m in the late nineteenth century to 13 m relative to mean lower low water (MLLW) today (Table 1 and Figure 2). The channel is deeper at the mouth of the river and the six miles (9.7 km) of the inboard side of the Mouth of Columbia River is maintained at 14.6-m (48-foot) depth, while the six miles (9.7 km) on the outboard side are maintained at 16.8-m (55-foot) depth (USACE, n.d.).

Available maps created between 1792 and 1879 depict a river mouth with one, and sometimes two, channels that meandered over annual and decadal time scales and changed depth frequently. Uncertain bathymetry, combined with strong waves and large currents (rivers + tides), produced hazardous conditions that caused many shipwrecks (including two U.S. Navy ships—the USS Peacock and the USS Shark) and earned the region the name "Graveyard of the Pacific." The clear hazard, and the degradation of the available channel by the early 1880s, motivated the U.S. Congress to allocate money for improvement of the channel entrance (Public Acts of the 47th Congress, 1882; Hickson & Rodolf, 1950; Lockett, 1959; Kidby & Oliver, 1965). The South Jetty, started in 1885 and completed in 1895, extended 4.5 miles (7.2 km) into the ocean and was initially built to provide a 30-foot (9.1-m)-deep channel at the entrance. By 1896, only a 29-foot (8.8-m)-deep channel was available at the bar, and by 1898, two channels had formed due to the continued accretion along the Clatsop Spit. To address such problems and accommodate increasing ship sizes, The Rivers and Harbors Appropriation Act of 1905 authorized a 40-foot (12.2-m)-deep, ½-mile (0.8-km)-wide channel at the mouth. This led to an extension of the South Jetty to 7 miles (11.2 km) in 1913 and the construction of the 3-mile (4.8-km)-long North Jetty (completed in 1917). By 1931, due in part to the deterioration of the South Jetty, Clatsop Spit migrated north and west. Several projects were undertaken to alleviate this condition, including the rehabilitation of the South Jetty from 1931–1936, rehabilitation of the North Jetty from 1938–1939, construction of Jetty "A" normal to the North Jetty, and the installation of four pile dikes along the south shore of Sand Island in 1939 (Hickson & Rodolf, 1950; Lockett, 1959). Further deepening of the entrance channel was authorized in 1954, and further deepening of the estuary and river was authorized in 1962 and 1999 (Table 1). The construction of the jetties is mostly responsible for moving in excess of 250 million cubic meters of sand seaward (Sherwood et al., 1990).

Table 1
Acts of Congress Authorizing Expenditures for Modification of the Columbia River Channel and Mouth of the Columbia River

	Mouth of the Columbia River	
1882	Public Acts of the 47th Congress	30′ (9.1-m) depth
1905	River and Harbor Act	40′ (12.2-m) depth, ½-mile (0.8-km) width
1954	River and Harbor Act	48′ (14.6-m) deep, ½-mile (0.8-km) width
Columbia River Channel		
1878	Act to Improve Rivers and Harbors	20′ (6.1-m) depth
1899	Rivers and Harbors Appropriation Act	25′ (7.6-m) depth
1912	River and Harbor Act	30′ (9.1-m) depth, 300′ (91-m) width
1930	River and Harbor Act	35′ (10.7-m) depth, 500′ (152-m) width
1962	Rivers and Harbors Act	40′ (12.2-m) depth, 600′ (183-m) width
1999	Water Resources Development Act	43′ (13.1-m) depth

Note. Depth relative to mean lower low water (Hickson, 1961; Kassenbaum, 2011; Lockett, 1959).

3. Materials and Methods

3.1. Modern and Historic Data

Extensive nineteenth-century hydrological and tidal records are available for the LCRE (Talke & Jay, 2013, Jay et al., 2010, Naik & Jay, 2005). The records serve to (a) characterize the tidal progression from the Pacific Ocean to Bonneville Dam, (b) define the elevation versus flow rating curve in the Portland area during the late nineteenth century, (c) elucidate discharge patterns of the late nineteenth century, and (d) provide boundary conditions for the historic model. By comparing nineteenth century data with modern data, we can analyze changes to boundary conditions and secular changes in water levels and tides. Table 2 details the historical records used in this study, and Table 3 details the modern data.

A long series of tide records at Astoria from 1853–1876 has been recovered (Talke & Jay, 2017), as well as tide logs from 13 stations in the LCRE, an estuary survey in 1868, and a river survey in 1877 during low flow conditions (Table 2). Water levels were extensively quality assured to eliminate data with measurement and timing errors (Helaire, 2016), and short series were discarded. After quality assurance, only six short-term records (Table 2) were of sufficient quality to perform a tidal harmonic analysis using robust least squares fitting (Leffler & Jay, 2009; Pawlowicz et al., 2002). The constituent amplitudes and phases obtained from harmonic analysis were later used to calibrate and validate the model. The same approach is used with modern data (Table 3).

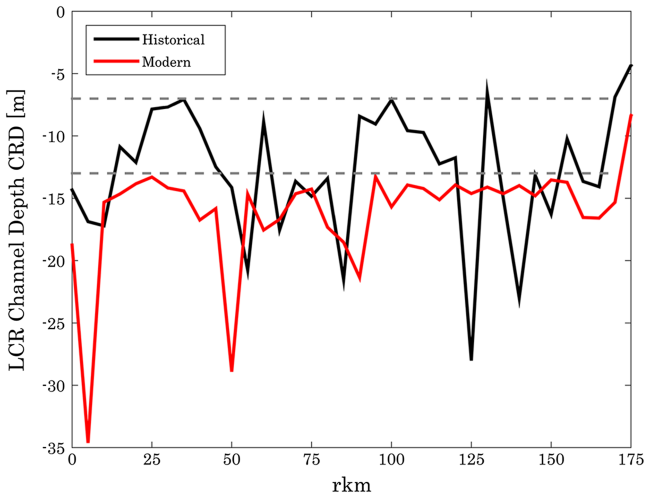

Figure 2. Lower Columbia River (LCR) Estuary channel depth in the historical (late nineteenth century) and modern period relative to North American Vertical Datum of 1988. The dotted gray lines indicate the approximate historical and modern controlling depth.

Daily water level readings from the Willamette River at Portland (OR) have been measured nearly continuously since at least 1876, first at Stark Street and later at the nearby Morrison Street Bridge. Multiple copies of nineteenth- and early twentieth-century records exist, including at the City of Portland archives (1880–1914), the National Weather Service office in Portland (1876, 1879–1898), the U.S. Signal Service, and U.S. Weather Bureau archives at the National Centers for Environmental Information (1879–1972; https://www.ncdc.noaa.gov/EdadsV2) and a series of reports compiled by the United States Weather Bureau (1893). Graphical records of stage height from 1876 to 1878 were found and digitized from the Annual Report of the U.S. Army Corps, 1879. For analysis of modern water levels, mean, minimum and maximum daily water levels are available from 1972, and hourly (or better) readings are available 1986 to present from USGS and NOAA, though there are gaps.

Daily discharge records for the Columbia River at The Dalles for 1878 to the present are available from USGS (http://waterdata.usgs.gov/usa/nwis/uv?14105700). Fragmentary discharge estimates were made for the Willamette River at Albany, OR, between 1878 and 1888 (39% percent complete) and continuously from 1892 onward (USGS Station # 1417100). Water level in Portland is dependent on Columbia and

Table 2
Nineteenth-Century Water Level and Discharge Data

Station	River	Rkm	Type	Dates
[a]Fort Stevens, OR	CR	2.6	High/low tide	15 Jul to 15 Sep 1868
[a]Astoria, OR	CR	24	Hourly water level	1870 to 1876
[a]Cathlamet, WA	CR	60	High/low tide	12 Sep to 15 Oct 1877
[a]Oak Point, WA	CR	87	High/low tide	12 Sep to 15 Oct 1877
[a]Rainier, OR	CR	108	High low tide	12 Sep to 15 Oct 1877
[a]Vancouver, WA	CR	168	High/low tide	12 Sep to 15 Oct 1877
[a]Warrendale, OR	CR	228	30–60 min, 18–20 hr/day	13 Sep to 10 Oct 1877
[b]Morrison Br.	WR	12.8	Daily water level	Jan 1876 to Jun 1878
[c,d]Morrison Br.	WR	12.8	Daily water level	1879 to 1898
[b]Albany, OR	WR	190	Daily water level	Jun 1877 to Jun 1878
[e]Albany, OR	WR	190	Daily discharge	1878–1888 (gaps); 1892 to date Dd
[f]The Dalles, OR	CR	305	Daily discharge	1878 to present

Note. CR = Columbia River; WR = Willamette River; MSB = Morrison Street Bridge, Portland.
[a]Digitized tide logs (USC&GS, 1877). [b]Discharge estimate (USACE, 1915). [c]Daily water level at EV2 database (https://www.ncdc.noaa.gov/EdadsV2). [d]United States Weather Bureau (1879). [e]United States Weather Bureau (1878). [f]Henshaw and Dean (1915).

Willamette River discharge, as well as the tidal amplitude. To provide a more complete Willamette River flow record, an estimate of the Willamette River discharge in the nineteenth century was determined through an iterative model using inputs of river discharge, water level, and downstream tidal range.

3.2. Bathymetry

In our model, we use the river channel and floodplain bathymetry from a merged data set of multibeam surveys and LiDAR-derived elevations (USACE, 2010). Continental shelf depths were obtained from The National Geophysical Data Center digital elevation model (DEM) (National Geophysical Data Center, 2003).

The majority of the bathymetry and topography data used to produce our historical DEM were extracted from hydrographic surveys made by the U.S. Coast and Geodetic Survey (USC&GC; present-day National Geodetic Survey) between 1868 and 1901. The digitized and georeferenced surveys are tied horizontally to the North American Datum of 1983 and vertically to North American Vertical Datum of 1988 (Burke, 2010). These surveys typically measured the topography below MLLW. To obtain intertidal flats and floodplain bathymetry, we integrate modern Lidar measurements (USACE, 2010) into the historical DEM, after removing modern landscape features such as roads and dikes. Because vertical land motion due to tectonics is small in the tidal river (Burgette et al., 2009), the bathymetry of extant wetlands is likely well estimated. Subsidence due to oxidation of soil in diked regions causes an unknown error in floodplain bathymetry (in practice, this is compensated for by using a larger friction coefficient; see section 4 and supporting

Table 3
Modern Water Level and Discharge Data

Station	River	rkm	Type	Dates	Source	Station ID
[a]Hammond, OR	CR	14.5	10-min water level	1–30 Sep 2005	NOAA	9439011
[a]Astoria	CR	28	10-min water level	1–30 Sep 2005	NOAA	9439040
[a]Skamokawa	CR	54.2	10-min water level	1–30 Sep 2005	NOAA	9440569
[a]Longview	CR	106.7	10-min water level	1–30 Sep 2005	NOAA	9440422
[a]Saint Helens	CR	138.6	10-min water level	1–30 Sep 2005	NOAA	9439201
[a]Vancouver, WA	CR	171.1	10-min water level	1–30 Sep 2005	NOAA	9440083
[b]Morrison Br.	WR	12.8	10-min water level	1–30 Sep 2005	USGS	14211720
[b]Morrison Br.	WR	12.8	Hourly discharge	1–30 Sep 2005	USGS	14211720
[c]Bonneville	CR	234	Hourly discharge	1–30 Sep 2005	USACE	

Note. CR = Columbia River; NOAA = National Oceanic and Atmospheric Administration; WR = Willamette River; USACE = United States Army Corp of Engineers; USGS = U.S. Geological Survey.
[a]NOAA (https://tidesandcurrents.noaa.gov/map/index.html). [b]USGS (https://waterdata.usgs.gov/nwis/). [c]http://www.fpc.org/river/flowspill/FlowSpill.asp.

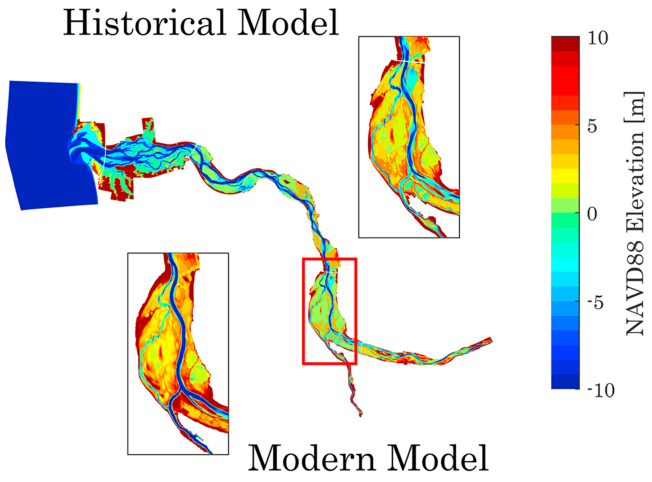

Figure 3. Model depths for historical model. (inset) Model depths for modern model. NAVD88 = North American Vertical Datum of 1988.

information). Outside of the immediate river mouth, continental shelf bathymetry was defined using modern surveys; similarly, bathymetry upstream of rkm 219 and upstream of Portland (OR) is obtained from modern measurements. Our analysis of Portland water levels (see section 4) suggests that before 1900, significant overbank flow occurred for river discharges of greater than ~20×10^3 m^3/s. We estimate the spatially variable levee height implied by a 20×10^3-m^3/s discharge by analyzing the water surface profile from Bonneville (rkm 230) to the ocean compiled by the U.S. Army Corps for historical floods from as early as 1876 (USACE, 1963). The USACE flood profile contains an estimate of flood stage along the river channel from Bonneville to the estuary. The resulting DEM was checked and modified using georeferenced nineteenth-century LCRE topography sheets (Burke, 2010), which provide information about the placement of historical wetlands, channels, forests, and other ecotypes. Where available, additional navigation maps, particularly of the Willamette River, were recovered and digitized (McIndoe & Thomson, 1911; Thorn, 1888). The resulting DEM represents nineteenth-century conditions as well as possible with available data (see Helaire, 2016).

3.3. Model and Computational Grid

Simulations are run on the Delft3D platform (Roelvink & Van Banning, 1995) and are based on a modified version of the grid used in Elias et al. (2012) that had been expanded to include floodplains and extends the domain to the head of tides. Since we are primarily interested in the tidal river landward of salinity intrusion, we use a barotropic (depth-averaged) approach. Nonetheless, to define tidal propagation through the estuary, we extend the grid 30–35 km into the open ocean (Figure 3). The tidal amplitude and phase of the oceanic tides of the eight largest harmonic constituents (Tables 4 and 5) are defined at the extreme southwest and northwest points on the ocean boundary and are obtained from the Oregon State University Tidal Prediction Software tide model using the Pacific Northwest regional submodel (Egbert & Erofeeva, 2002). Neumann boundaries are applied on the north and south edge of the coastal boundary (surface slope $dh/dx = 0$).

The model segment representing the estuary and fluvial domain extends upstream from the mouth of the Columbia River to Bonneville, OR (CR rkm 234), and includes the Willamette River from the confluence with the Columbia River to a discharge boundary at the head of tides at Oregon City, OR (WR rkm 41). The model grid extends from the river channel far enough to model 20 m of inundation relative to North American Vertical Datum of 1988, sufficient to model a historical event such as the flood in June 1894. The model has a grid resolution varying from 2 km in the ocean to 50 m in some of the smaller channels. To make use of multiple cores on our workstation and decrease computation time, we decomposed both the historical and modern model into different subdomains, using well-validated functionality (Hydraulics, 2006; Roelvink & Van Banning, 1995) that has been previously applied to the Columbia River Estuary (i.e., Elias et al., 2012) and in numerous other studies (e.g., Martins et al., 2001; Sandbach et al., 2018; Sleigh et al., 1998; Tanaka et al., 2011; Wang et al., 2012). In domain decomposition boundary conditions at subdomain boundaries are handled internally, and the user needs only specify the grid geometry at connection points correctly. The grid is partitioned automatically in the traditional implementation of domain decomposition. In the Delft3D implementation of domain decomposition, the grid is partitioned manually. Small differences occur between models with and without domain decomposition (Hydraulics, 2006); however, since we calibrate our model with data from each domain, we are confident that any artifacts from model setup are negligible. We used five subdomains in the modern model with 242,382 total grid cells, and six subdomains in the historical model with 334,629 total grid cells. The larger number of cells in the historical model was needed to accurately model overland flow and necessitated the additional subdomain. The differences in grid resolution stem almost entirely from the underlying data DEMs employed for the two periods. Specifically, the historical bathymetry (Burke, 2010), is much coarser than the modern bathymetry (USACE, 2010), and there is no point in using a historical grid with a resolution not supported by the underlying DEM. Since we have data within each subdomain except the ocean domain (Tables 2 and 3), we were able to validate that any small errors that might occur at the connection points between domains did not materially affect results and could be neglected.

Table 4
Tidal Constituents for Historical Model at the Ocean Boundary

	Southwest			Northwest	
Constituent	Amplitude (m)	Phase (°)	Constituent	Amplitude (m)	Phase (°)
M_2	0.890	232.57	M_2	0.896	232.89
S_2	0.248	259.63	S_2	0.252	260.48
N_2	0.187	206.50	N_2	0.190	207.44
K_2	0.066	249.86	K_2	0.067	251.34
K_1	0.426	240.20	K_1	0.426	239.74
O_1	0.265	224.60	O_1	0.263	224.58
P_1	0.131	235.96	P_1	0.131	236.05
Q_1	0.047	213.58	Q_1	0.047	214.40

Domain decomposition is also useful in the development of the modern model because spatial changes in the resolution of the model grid are needed in several areas. An example is in tributary channels like the Willamette River and Multnomah Channel. Given the extensive changes in shoreline and the amount of filling and diking, it is logical that domains are handled somewhat differently in the historical and modern models. Specifically, due to an extensive system of levees placed in the Columbia River, a large amount of flow is confined to narrower channels (the extent of levees in the LCRE is depicted in Avi, 2017). Some differences in the grids are due to the realignment of the river channel. An extreme example is Swan Island on the Willamette River. In the late nineteenth century, Swan Island was an island within the Willamette River, with the main Willamette River navigation channel flowing to the east side of the island (Thorn, 1888). In the present configuration, Swan Island is a peninsula with the main Willamette River navigation channel flowing on the west side of the former island.

The grids are divided into subdomains representing different reaches of the coupled ocean-river system. The domain decomposition functionality works best when the subdomains are of approximately the same size and complexity. Given the differences in shorelines and floodplain extent, this dictates the use of different domain decompositions in the modern and historical model. The modern model has an ocean subdomain which is 58 km from north to south and extends 30–35 km from the coast. The next subdomain represents the entrance to the Columbia River and the estuary up to Columbia River rkm 50. The lower reaches of the tidal river are represented by a subdomain from rkm 50–136 on the Columbia River. Further upstream is a subdomain representing the Portland/Vancouver area, including the Columbia River from rkm 136–176 and the tidally influenced segment of the Willamette River, from the confluence with the Columbia River to the extent of tidal influence at Oregon City (rkm 41). The final subdomain represents the Columbia River upstream of the dredged shipping channel (USACE, n.d.) and stretches upstream from rkm 176 to Bonneville, OR (rkm 234).

The historical model has an ocean subdomain that is 50 km from north to south and extends roughly 30 km into the ocean. The ocean domain, which includes the most seaward 14 km of the Columbia River, is refined compared to the ocean domain in the modern model because it inherits some of the grid resolution of the river channel that projects into the ocean. Because frictional effects are small in the deep water of the coastal domain, the different resolution between modern and historical models makes little difference in results (and, as stated before, our region of interest is upstream of Astoria, which is located approximately 25 km from the coast. Upstream of the ocean subdomain is a subdomain representing the Columbia River from rkm 14–52. The lower reaches of the tidal river are represented by a subdomain from rkm 52–140. The Portland/Vancouver area is represented by two subdomains. One subdomain includes the Columbia River from rkm 140–176 and the Willamette River from the confluence with the Columbia River, upstream to Willamette rkm 7. The other subdomain represents the Willamette River from rkm 7 to the end of tidal influence at Oregon City (rkm 41). The final subdomain models the upper reaches of the tidal Columbia River from rkm 172 to Bonneville (rkm 234).

Table 5
Tidal Constituents for Modern Model at the Ocean Boundary

	Southwest			Northwest	
Constituent	Amplitude (m)	Phase (°)	Constituent	Amplitude (m)	Phase (°)
M_2	0.883	231.4	M_2	0.889	232.2
S_2	0.247	258.8	S_2	0.253	260.2
N_2	0.187	206.0	N_2	0.190	207.3
K_2	0.066	249.6	K_2	0.067	251.3
K_1	0.424	239.6	K_1	0.428	239.5
O_1	0.264	224.2	O_1	0.264	224.3
P_1	0.131	235.4	P_1	0.131	236.0
Q_1	0.047	213.6	Q_1	0.047	214.4

The historical and modern models have similar run parameters. The water in the domain representing the coastal ocean is set to 15 °C, 31 parts per thousand (ppt) salinity, and 1,000-kg/m^3 density. The river discharge from the Willamette River and Columbia River is set to 20 °C, 0-ppt salinity, and 1,000-kg/m^3 density. The background horizontal eddy viscosity and eddy diffusivity is set to 10 and 1 m^2/s, respectively. A time of step of 0.5–1.0 min was used depending on the model run. Both the modern and historical models use a single vertical layer. Since the river is energetic and we are interested in flood conditions, the assumption of well-mixed conditions is reasonable. A depth variable Chézy coefficient is applied, as described below.

3.4. Calibration

The historical and modern models were calibrated to reproduce tidal constituents along the channel during low flow conditions and to reproduce MWL, tide range, mean high water, and mean low water in Portland during a variety of flow conditions (Tables 6 and 7). Small-scale and subgrid-scale roughness elements such as vegetation in the floodplain, debris such as log jams, or small-scale morphodynamic features are known to affect frictional drag (e.g., Arcement & Schneider, 1989). To account for floodplain drag, we use a depth-dependent roughness parameterization in which the Chézy friction coefficient varies depending on whether it is above or below MLLW. A similar approach has been used before to model tidal amplification and asymmetry (e.g., Nicolle & Karpytchev, 2007). During calibration (section 4.1), we first considered low river discharge conditions and calibrated the historical model to match September–October 1877 tides and the modern model to reproduce August–September 2005 tides. Next, we altered floodplain friction until the rating curve for water level versus flow matches measurements (section 4.2). Our simplified approach effectively assigns one roughness value to vegetation in each domain and provides insight into how resistant to flow the historical floodplain was.

In both the historical and modern models, the river channels have lower roughness—as indicated by a higher Chézy coefficient ($m^{1/2}/s$)—than the floodplains, and the upstream river channels have higher roughness (lower Chézy coefficients) than the estuary (Sandbach et al., 2018). In the channels (sand bedded throughout the entire system), bedforms are small (usually <0.5 m) and tidally reversing at the entrance, <1–2 m and seasonally reversing within the remaining reaches with salinity intrusion, but substantially larger upriver, up to 3–5 m in deep water. Both our models have spatially variable roughness but in different ways. In the modern model, channel roughness ranges from 55–96, compared to 25–50 for the historical model. Within the estuary in the modern model, a low roughness (large Chézy) of 96 was used, to account for the reduction in friction caused by salinity stratification (see Giese & Jay, 1989). In the historical estuary, a Chézy roughness of 50 was used. The larger roughness in the historical channel likely has some basis in fact. Compared to the modern channel, sand waves and other features were not regularly dredged historically. Moreover, the annual reports of the U.S. Army Corps regularly described shifting sand bars at the mouths of tributary rivers such as the Willamette and Cowlitz, as well as at the estuary mouth, features that may not be fully represented in the historical bathymetry. Finally, the shallower depth likely meant that salinity intrusion was less, which causes the effective friction to increase (Giese & Jay, 1989). We note that the roughness may also compensate somewhat for any inaccuracies in the historical bathymetry and datum; for example, since the bathymetry is a composite of different surveys between 1868 and 1901, it is possible that conditions changed over time.

Both models have higher floodplain roughness than channel roughness, based in part on the physical characteristics of the floodplain. Subtidal sand flats are found in the estuary (no vegetation and mostly sand but some fines) and freshwater marshes are observed in most peripheral areas (salt marshes occur very close to the entrance). Larger vegetation is observed further upriver, mostly now brushy vegetation, but with some remnant forested swamps (Jay et al., 2016). Forested swamps were much more extensive historically before they were logged in the early twentieth century. They were very rough, somewhat akin to a cypress swamp in the SE United States. In general, about 60–80% of vegetated wetlands have been lost (Marcoe & Pilson, 2017). These observations reinforce the use of variable roughness and the need to use historical data to validate the model.

3.5. Simulations

Many numerical simulations were run to quantify the landward progression of the tide, upstream water levels, and the interaction between tides and river discharge (Tables 6 and 7). Constant discharge simulations were used to estimate the equilibrium response of water levels to stationary forcing. In addition, the response of both the modern and historical models to a large spring freshet was simulated by applying a Gaussian hydrograph (standard deviation [σ] = 30 days) with a duration of 179 days (4 March to 30 August 2005), a baseline amplitude of 2.5×10^3 m^3/s, and a peak amplitude of 25×10^3 m^3/s. This peak discharge, though typically not observed in the modern system, was exceeded 5 times between 1858 and 1894 and is approximately representative of the 1880 spring freshet.

Table 6
Simulations Run on the Historical Model

Run type	Columbia River discharge	Willamette River discharge	Duration
Tidal decay	The Dalles estimated	Portland estimated	31 Aug to 18 Oct 1877
Water level	2,500 m^3/s constant	250 m^3/s constant	11 Apr to 11 Nov 1876
Water level	5,000 m^3/s constant	250 m^3/s constant	11 Apr to 11 Nov 1876
Water level	10,000 m^3/s constant	250 m^3/s constant	11 Apr to 11 Nov 1876
Water level	15,000 m^3/s constant	250 m^3/s constant	11 Apr to 11 Nov 1876
Water level	20,000 m^3/s constant	250 m^3/s constant	11 Apr to 11 Nov 1876
Water level	25,000 m^3/s constant	250 m^3/s constant	11 Apr to 11 Nov 1876
Water level	30,000 m^3/s constant	250 m^3/s constant	11 Apr to 11 Nov 1876
Flood pulse	Gaussian 25,000 m^3/s max	250 m^3/s constant	17 Feb to 19 Oct 2005

3.6. Interpretation

The tidally averaged momentum and mass balance in open channel flow can be approximated using the St. Venant equations (Cunge et al., 1980), under the assumption that flow is sectionally integrated, density is constant, and the vertical pressure distribution is hydrostatic:

$$\frac{1}{g}\frac{\partial u}{\partial t}+\frac{u}{g}\frac{\partial u}{\partial x}+\frac{\partial h}{\partial x}=S_O-\frac{\tau_0}{\rho g R}, \tag{1}$$

$$\frac{\partial Q}{\partial t}+b\frac{\partial h}{\partial t}=0 \tag{2}$$

On the left-hand side of equation (1), g is gravitational acceleration, u is along channel velocity, t is the time scale, x is the along channel direction, and h is the elevation above mean surface elevation. The left-hand side of equation (1) is balanced by the difference between the surface slope, S_o, and the friction slope, S_f, which is a function of the water density, ρ; the bed stress, τ_0; and the hydraulic radius, R. The hydraulic radius, R, is approximately equal to the depth in a wide and relatively shallow river such as the Columbia River. In equation (2), Q is the along channel discharge, and b is the channel width. As key parameters such as bed friction and depth change, the relative magnitude of each term in the equation changes, leading to measurable differences in the slope, phase speed, and dispersion of a flood wave. To help interpret and understand how altered bathymetry and bed friction have changed river slope and flood waves, we therefore use model results to estimate terms in equation (1) (see section 4).

Variations in dh/dx (equation (1)) over time must be balanced by changes to the friction slope, S_f. The friction slope can depend on many factors, but in the simplest case, friction relates directly to the velocity and Chézy roughness, such that a decrease in roughness (higher Chézy coefficient) causes a decrease in the friction slope.

$$\tau=\frac{\rho u^2}{C} \tag{3}$$

Table 7
Simulations Run on the Modern Model

Run type	Columbia River discharge	Willamette River discharge	Duration
Tidal decay	Bonneville measured	Portland measured	31 Aug to 18 Oct 1877
Water level	2,500 m^3/s constant	250 m^3/s constant	11 Apr to 1 Aug 2005
Water level	5,000 m^3/s constant	250 m^3/s constant	11 Apr to 1 Aug 2005
Water level	7,500 m^3/s constant	250 m^3/s constant	11 Apr to 1 Aug 2005
Water level	10,000 m^3/s constant	250 m^3/s constant	11 Apr to 1 Aug 2005
Water level	12,500 m^3/s constant	250 m^3/s constant	11 Apr to 1 Aug 2005
Water level	15,000 m^3/s constant	250 m^3/s constant	11 Apr to 1 Aug 2005
Water level	25,000 m^3/s constant	250 m^3/s constant	11 Apr to 1 to 1 Aug 2005
Flood pulse	Gaussian 25,000 m^3/s max	250 m^3/s constant	17 Feb to 19 Oct 2005

Table 8
Modern Coefficients and Exponents for Tidal Datums at Morrison Street Bridge (1998–2008)

Coefficient	LLW	MWL	HHW	Exponents	
a_0	−1.06288	−0.652115	0.132244	m_1	0.95
a_1	0.655633	0.59757	0.493093	m_2	1.2
a_2	0.21758	0.197587	0.174479	m_3	0.7
a_3	0.09608262	0.138429	0.2016		

Note. HHW = higher high water; LLW = lower low water; MWL = mean water level. Units are in meters; datum is CRD.

In equation (3), τ is the bed stress, C is the Chézy friction coefficient, ρ is the water density, and u is the channel velocity.

Jay et al. (2016) developed a modified rating curve to predict how water levels in the LCRE respond both to river discharge and to the time-varying frictional interaction of river flow and oceanic tides. Applied to the water level series in Portland, we must include terms to account for water level variations caused by flow from the Willamette River (Q_{WR}) and the Columbia River. Hence, the Jay et al. (2016) equation for water level (WL) becomes

$$WL = a_0 + \underbrace{a_1(Q_{\mathrm{WR}})^{m1}}_{\text{Willamette River}} + \underbrace{a_2(Q_{\mathrm{TD}})^{m2}}_{\text{Columbia River}} + \underbrace{a_3\left(\frac{T_{\mathrm{RA}}^2}{(Q_{\mathrm{TD}}+Q_{\mathrm{WR}})^{m3}}\right)}_{\text{tides}}, \quad (4)$$

where the subscript WR denotes the Willamette River, the subscript TD refers to flow measurements at The Dalles, and T_{RA} is the greater diurnal tide range at Astoria (OR), obtained from tide prediction software (Pawlowicz et al., 2002). The final term models the interaction between ocean tides and river discharge. The constant a_i are coefficients, and m_i are exponents, and are found by a nonlinear regression technique that minimizes the error between water level observations and predictions.

While equation (4) is sufficient to statistically model modern water levels, an additional term is needed in historical data to account for the roll-off in the rating curve that occurs once overbank flow is initiated. We model overbank flow with an additional power law term, such that

$$WL = a_0 + \underbrace{a_1(Q_{WR})^{m1}}_{\text{Willamette River}} + \underbrace{a_2(Q_{TD})^{\mathrm{m2}}}_{\text{Columbia River}} + \underbrace{a_3\left(\frac{T_{RA}^2}{(Q_{TD}+Q_{WR})^{m3}}\right)}_{\text{tides}} + \underbrace{a_4\max\left(\frac{Q_{WR}+Q_{TD}}{Q_{CRIT}}|1\right)^{m2}}_{\text{overbank flow term}}. \quad (5)$$

For flows below a critical discharge (Q_{Crit}) of 20×10^3 m^3/s, the "overbank flow term" reduces to the constant a_4; above the critical discharge, the term exerts an influence on the water level curve and models the kink in the observed rating curve caused by historical overtopping (see section 4). The coefficients and exponents for the modern period (equation (4)) are given in Table 8, and those for the historical period (equation (5)) are given in Table 9.

The most obvious difference in the coefficients between modern and historical periods is that a_0 was substantially larger historically (Tables 8 and 9). However, this is a byproduct of the inclusion of the overbank term. Below 20×10^3-m^3/s discharge in the historical model, the overbank term simply reduces to the coefficient a_4. Under these conditions, the constant term is −0.12 and is smaller than modern MWL. The second difference is that the modern flow exponents for the Columbia River and Willamette River, m_1 and m_2, are larger than the historical flow exponents. This indicates differences in the shape of the rating curve in historical and modern periods.

4. Results

4.1. Tides

Analysis of tide records and model results suggests that semidiurnal and diurnal constituents were smaller historically than they are today over most of the LCRE. In the historical model, the semidiurnal M_2 amplitude peaked at 0.95 m at rkm 25 and dropped steadily up to rkm 165, where a more precipitous drop in amplitude occurred (Figure 4). In the modern model, M_2 amplitude also peaks near rkm 25, with an amplitude (1.03 m) that is 8.4% higher than in the historical model. M_2 amplitude then remains nearly constant for 25 km upstream to Wauna and decreases steadily thereafter. The largest difference in M_2 between historical and modern simulations occurs at rkm 61 (Figure 4). Both models show a precipitous decrease in tide magnitudes near the confluence with the Willamette River but at slightly different locations (rkm 165 historically

Table 9
Historical Coefficients and Exponents for Historical Daily Water Level at Morrison Street Bridge

Coefficients		Exponents	
a_0	2.53	m_1	0.45
a_1	0.48	m_2	0.78
a_2	0.83	m_3	1.38
a_3	0.33		
a_4	−2.65		

Note. Units are in meters; datum is CRD.

and rkm 170 in the modern model). Reasons include (a) an abrupt change in channel depth immediately downstream of Vancouver, with a location that is slightly different in the modern model due to the Port of Vancouver/Portland, (b) an increase in roughness further landward, due to a lack of dredging (modern system), and (c) the junction with the Willamette River and the historical bar that formed there.

Similar to the M_2 tide, the S_2 tide is amplified at the entrance, likely due to bathymetric convergence. Also similar to the M_2 tide, the S_2 tide is also damped more heavily in the historical model than the modern model (Figure 4). The S_2 tide has a peak amplitude of 0.255 m at around rkm 25 in the historical model, similar to M_2. In the modern model, the peak amplitude is larger (0.346 m) and peaks further upstream (rkm 35). Like M_2, the S_2 amplitude steadily decreases upstream of the amplitude peak until there is a large drop in amplitude near Vancouver (historical, rkm 165; modern, rkm 170). The K_1 tide is also damped more in the historical model than the modern model. In the historical model the K_1 peak amplitude is 0.31 m, compared to 0.41 m in the modern model. The O_1 tide, conversely, has similar behavior in the historical and modern model. The O_1 tide has an amplitude of 0.27 m at the entrance of the channel in both the historical and modern models.

For low flow conditions, the root-mean-square error (RMSE) between measured and modeled M_2 tides was 0.055 and 0.057 m across all gauge stations for the historical and modern model, respectively (Tables 2 and 3). The difference between modeled and measured constituents was slightly larger in the historic model than the modern model (Table 10), likely reflecting the different time period of harmonic analysis of nineteenth-century data, but also possibly occurring due to the greater probability of timing and transcription errors in historic field data (see, e.g., Zaron & Jay, 2014). We note that the available late nineteenth- and early twentieth-century bathymetric and water level measurements are not synoptic. They were collected over a 40+-year period, during which time large modifications were made to the channel and floodplain. Thus, the modeled topography and bathymetry represent a system that never actually existed in the form modeled but which is typical for the time period and which represents historical processes.

4.2. Changes in MWL and Discharge

MWLs in the Portland/Vancouver area have changed substantially over the last 150 years, particularly between April and September (Figure 5). For example, water levels in June from 1879 to 1898 averaged more than 3 m higher than during 1989 to 2008 (Figure 5c). A large part of the change can be attributed to the changing hydrograph at The Dalles (Figure 5a), which produces a smaller backwater effect in Portland during the seasonal spring freshet than before the onset of flow regulation circa 1970. Conversely, increased Columbia River discharge during winter months has slightly increased median water levels. Nonetheless, a portion of the reduced spring levels—as we show below—is likely attributable to a reduced river slope, such that the same river discharge results in a lower MWL today than in the past (as also suggested in Jay et al., 2010). The Willamette River hydrograph has also changed over time and influences the seasonality of mainstem Columbia River and Willamette River water levels to a lesser degree (Figure 5b), with a decrease in early spring flows (February to April) and an increase in summertime and early autumn flows (August to October). The Willamette changes likely influence the seasonality of average water-levels in Portland; the regression coefficients in Table 9 suggest a change of 0.05–0.18 m during spring for the MWL hydrograph. Since mean Willamette flows are an order of magnitude less than the Columbia River, effects of changed Willamette flow on MWL are restricted to the tidal Willamette between Kelly Point and Oregon City (Figure 5b; see also map on Figure 1).

A comparison of the modern and historical stage versus flow rating curves (Figure 6) during periods of low Willamette River flow demonstrates how system dynamics have changed over the past century. Most obviously, historical peak flows are much larger than modern peak flows, resulting in a larger range of flow conditions and overall larger backwater magnitudes. Moreover, the modern curve lies below the historical curve for all flows from 5–15 $\times 10^3$ m^3/s; therefore, the same river flow produces a lower river stage today (0.5 to 1 m lower) than historically, depending on discharge (see also Jay et al., 2010, for a similar result in Vancouver, WA). Also, the modern curve is slightly concave up, whereas the historical curve is

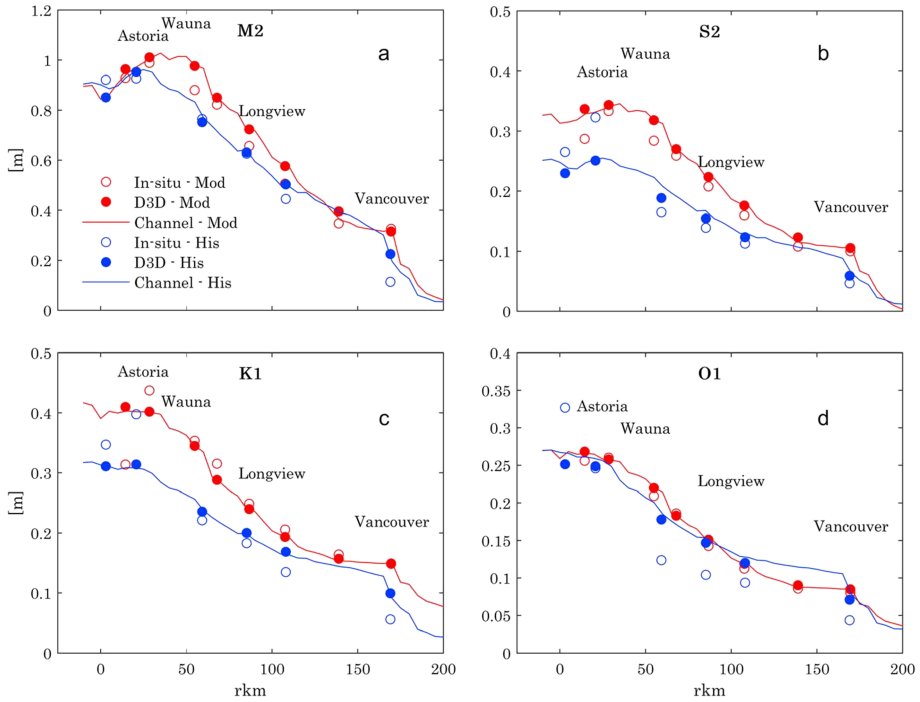

Figure 4. Spatial calibration of low flow event. Open dots represent in situ measurements, and filled dots represent model outputs (D3D = Delft3D) for stations. Solid line presents model output in river channel. (a) M_2, (b) S_2, (c) K_1, and (d) O_1. Blue = **historical**. Red = **modern**.

concave down. The shape of the historical curve reflects the effect of overbank flow; as water levels exceeded the natural levee height, water spread laterally and the rate of change in water depth per unit increase in discharge (dh/dQ) decreased. If the modern rating curve is assumed to be correct at high flows, it would intersect and exceed the historical rating curve around 20×10^3 m^3/s. If this were the case, modern flood control measures and navigation improvements would actually lead to larger water levels during floods, as has been suggested for the Mississippi River (e.g., Munoz et al., 2018). Not enough data are available to statistically evaluate the modern system response above 15×10^3 m^3/s; thus, it is unclear, without modeling, whether such an extrapolation to larger flows is valid. Hence, we next use modeling results to evaluate whether a "crossover" will occur or whether the modern system water levels are always below historical norms.

4.3. Modeled Flood Properties

Simulations confirm the qualitative expectation that inundation patterns due to a 25×10^3-m^3/s flood occurring over a 6-month period are different under modern and historical conditions (Figure 7), as might also be predicted by the rating curves (Figure 6). Interestingly, however, results suggest that historical peak flood levels are similar to (and slightly larger than) modern flood levels in the Portland/Vancouver metro area, despite a greater areal extent of flooding in the historical model (Figure 7). Consequently, the crossover predicted by extrapolating the rating curve in Figure 6 is not found in model results. However, the 0.5- to 1-m difference observed at low flows and caused by a decrease in the modern slope during those conditions has been largely erased. Thus, while levees included in the modern model prevent inundation of areas such as Sauvie Island (Figure 7), the resulting confinement of flow to the main channel (and decrease in off-channel storage) evidently increases water levels faster (larger dh/dQ) at elevated flows.

Table 10
RMSE Errors for the Four Largest Tidal Constituents in the Spatial Calibration of the Historical and Modern Model

Constituent	Historical	Modern
M_2	0.055	0.057
S_2	0.041	0.024
K_1	0.041	0.020
O_1	0.016	0.007

The difference in peak water level in the historical and modern models is spatially variable (Figure 8). Near the head of tides at Bonneville Dam, simulations suggest that historical water levels exceeded modern levels by as much as 2.6 m. Closer to the Portland/Vancouver metro

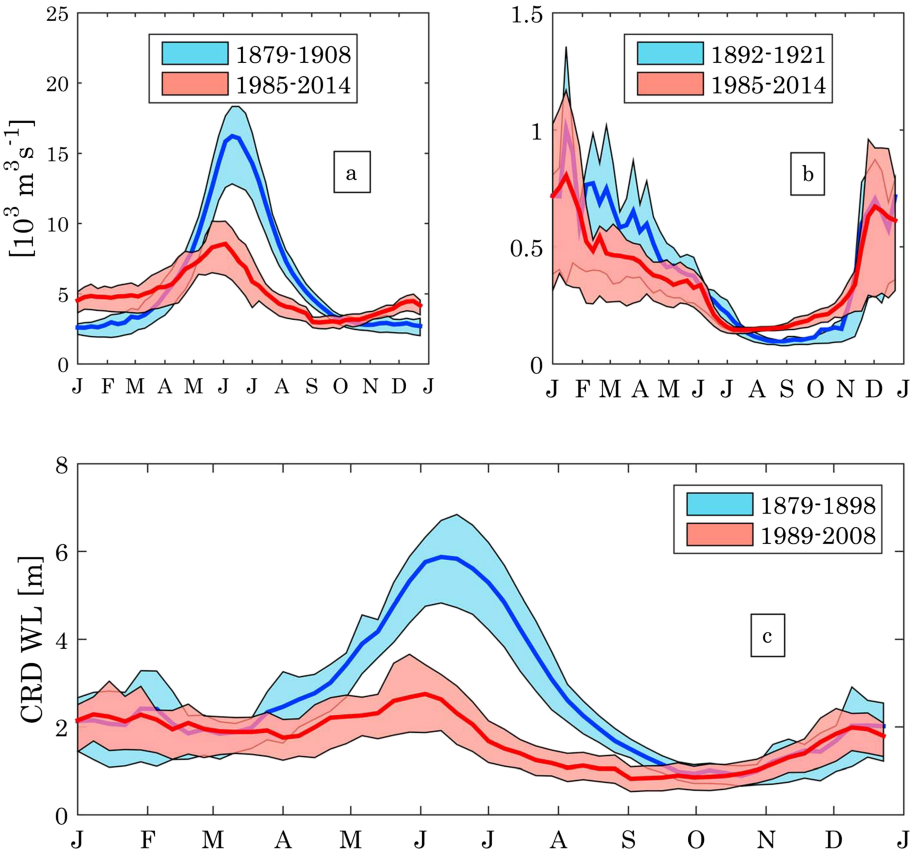

Figure 5. Solid lines are mean, fill area is 25–75% quantile. (a) Columbia River weekly mean discharge at The Dalles. (b) Willamette River weekly mean discharge at Albany. (c) Willamette River mean weekly water level at Morrison Bridge in Portland. CRD = Columbia River Datum; WL = water level.

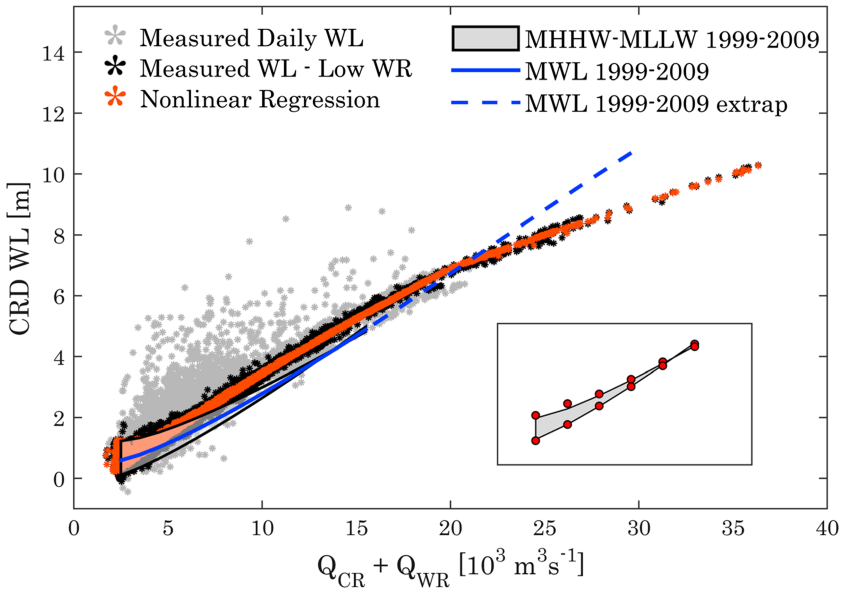

Figure 6. Comparison of historical and modern rating curve in Portland. Rating curve of water level at Stark Street/Morrison Bridge 1879–1898, rating curve restricted to low Willamette River discharge 1879–1898, nonlinear regression of restricted rating curve 1879–1898, nonlinear regression of HHW, MWL, and LLW for Morrison Bridge 1999–2009. The inset reproduces the LLW and HHW bounds for the modern period that are shown at the left around the mean MWL curve (blue) to highlight the concave up shape. CRD = Columbia River Datum; MHHW = mean higher high water; MLLW = mean lower low water; MWL = mean WL; WL = water level; WR = Willamette River.

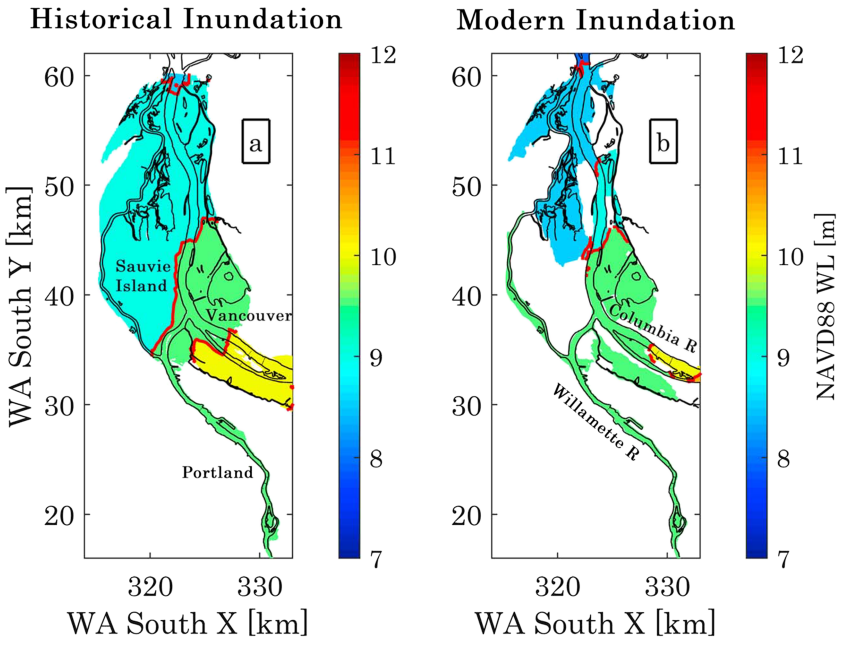

Figure 7. Inundation at the peak of the 25×10^3-m^3/s flood in the Portland/Vancouver metro area, overlaid with the modern coastline. (a) Historical model and (b) modern model.

area, water levels in the historical model still exceed the modern model but only by 0.1 m. Within this geometrically constrained reach, a crossover does occur at a much larger flow rate than is expected from extrapolation of the modern statistical model (Figure 6). At 30×10^3 m^3/s, simulations show that the modern water levels in Portland would be 9.81 ± 0.04-m elevation relative to Columbia River Datum, which is approximately 0.5 m higher than the expected historical river stage at this discharge (Figure 9). Though this flow level has been exceeded only once in peak flow records extending back to the 1850s (USGS Station 14105700), this observation does point out a vulnerability in the modern flood control system. Curiously, at 35×10^3-m^3/s discharge, equivalent to the June 1894 flood, simulations indicate that the modern water levels relax and are about the same as historical water levels in Portland, approximately 10 ± 0.04 m relative to CRD (Figure 9; see also Figure 6). Modern levee heights were built to withstand a flood close to 1894 levels; hence, once that level is reached, overbank flooding commences and the rating curve for modern flow changes.

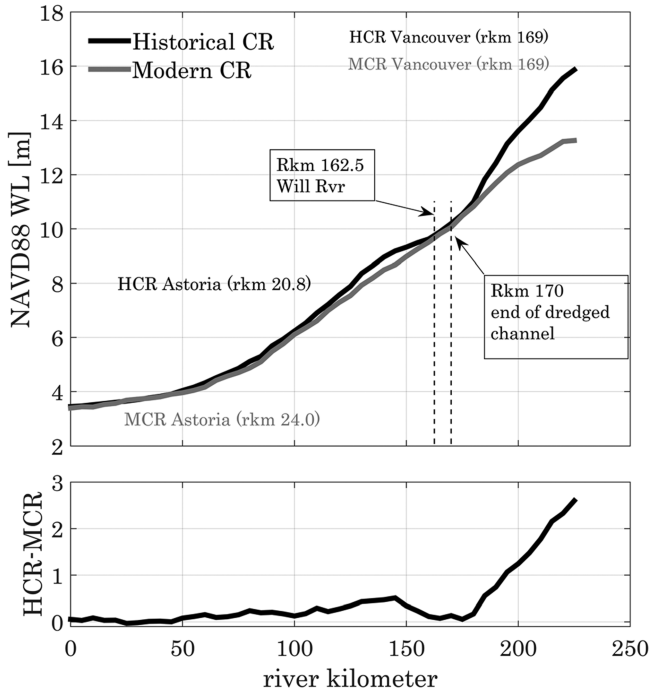

Figure 8. Peak total modeled water levels for 6-month simulated freshet in the historical and modern model. CR = Columbia River; NAVD88 = North American Vertical Datum of 1988.

Model results also suggest that tides were damped more under historical flood conditions than modern conditions (Figure 10). Hence, at the peak flow of a 25×10^3-m^3/s tide range decreased to below 1% of values at the mouth at rkm 130; in the modern model, the tides intruded to rkm 160 before dipping below the 1% threshold. Despite the difference in tidal damping in the historical and modern models, the total water levels downstream of Longview during the 25×10^3-m^3/s freshet are similar (Figure 8). The contributions to peak water levels due to tides and discharge have been altered in the modern case, with a larger tidal range compensated by lower baseline water levels. At Longview (rkm 108) there is only a 0.09-m difference between historical and modern peak water levels for the 25×10^3-m^3/s flood (6.69 m historically versus 6.60 m today; see Figure 10). At the peak of the flood, the modern tidal range is 0.24 m, compared to 0.05 m in the historical case. This indicates that a drop in

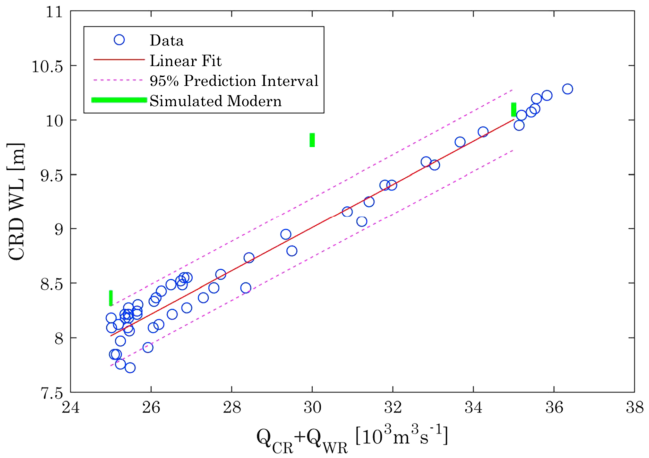

Figure 9. Portland water levels at Morrison Bridge for (green lines) modern model 25×10^3-, 30×10^3-, and 35×10^3-m^3/s constant flow simulations and (blue dots) river stage measurements 1879–1898. CRD = Columbia River Datum; WL = water level; WR = Willamette River.

baseline water level over the past 150 years at this flow rate is compensated by an increase in tidal range, which diminishes some of the flood control benefits of a deep channel. Farther downstream, in Cathlamet (rkm 60), peak water levels are much larger in the modern model, due to the increase in tide amplitudes since the nineteenth century; differences in MWL are relatively small, due the diminishing effect of river flow on water levels (Figure 10). The increased water levels around Cathlamet are driven by increases in the M_2 constituent, which are maximal around rkm 60 (Figure 4). In the estuary and lower tidal river, therefore, the spatial pattern of changed tide amplitudes is therefore quite significant in terms of flood risk, particularly since model results in other estuaries suggest that locations of large tide change are also regions of large changes to storm surge amplitudes (Familkhalili & Talke, 2016).

4.4. Channel Dynamics

To interpret water level trends, we note that diverse and sometimes conflicting changes have occurred over time. First, the channel and floodplain in the modern model are less rough than in the historical model (see supporting information). Initial evidence of the difference in roughness can be seen in the calibration of the tidal phase progression, where the historical model required a lower Chézy roughness value in the channel and floodplain than the modern model. Further, an examination of the topographical survey sheets (Burke, 2010) shows more vegetated floodplain than is the case today. This interpretation is supported by the findings of Marcoe and Pilson (2017), who found that the since the late nineteenth century 55% of the forested wetland and 68–70% of all wetlands have been lost. The larger historical bed roughness in both the channel and the floodplain produces a steeper surface slope and higher water levels at each point, for flows at and below 25×10^3 m^3/s. Effectively, a larger pressure gradient was required to drive the same flow historically, compared to today (third term in equation (1)). Additionally, the effect of friction is smaller in the deeper modern channel (Figure 2), because depth-averaged frictional effects are inversely proportional to depth (section 3.6 and equation (1)).

Reduction in roughness and friction effects causes tidal ranges to increase, while at the same time reducing MWLs. As a result, LLW has dropped, but only minor changes to higher high water have occurred; this effect is particularly evident during low and moderate flows (see also Jay et al., 2010; Ralston et al., 2019). The largest increases to higher high water occur where a maximum in M_2 change occurs; while a function of river flow, this occurs around rkm 60 (Figure 4). At high flows, modern levees constrain flow, limiting inundation but potentially increasing elevation in the main channel compared to historical conditions, since water cannot spread out laterally. Hence, several countervailing factors exist that can either decrease or increase modern water levels, compared to historical conditions. In locations in which overbank flow was once prominent (e.g., Figure 7), modern flow confinement tends to increase water levels during floods; where changes to lateral inundation are less extreme (such as upstream of Vancouver), frictional changes may be more important. Such opposing factors have led to different amounts of water level change in different reaches, as suggested by Figure 8.

We consider the issue from a kinematic point of view by considering the relationship between elevation and flow through a cross section; $h = Q/(ub)$, where h is the water surface elevation relative to the bed, Q is river discharge, b is width, and u is mean channel velocity. Taking the derivative with respect to flow, we find that the rate of change in water level with an incremental change of flow ($\frac{dh}{dQ}$) is

$$\frac{dh}{dQ} = \frac{1}{ub} - \frac{Q}{u^2 b}\left(\frac{du}{dQ}\right) - \frac{Q}{ub^2}\left(\frac{db}{dQ}\right), \tag{6}$$

where the first term on the right-hand side is a constant for a given flow rate (u) and geometry, and $\frac{du}{dQ}$ and $\frac{db}{dQ}$ are the rates of change of velocity and width, respectively, with an incremental change in flow. Since $\frac{db}{dQ}$ has decreased (for high flows at and below 25×10^3 m^3/s) in the modern model due to channelization and levee

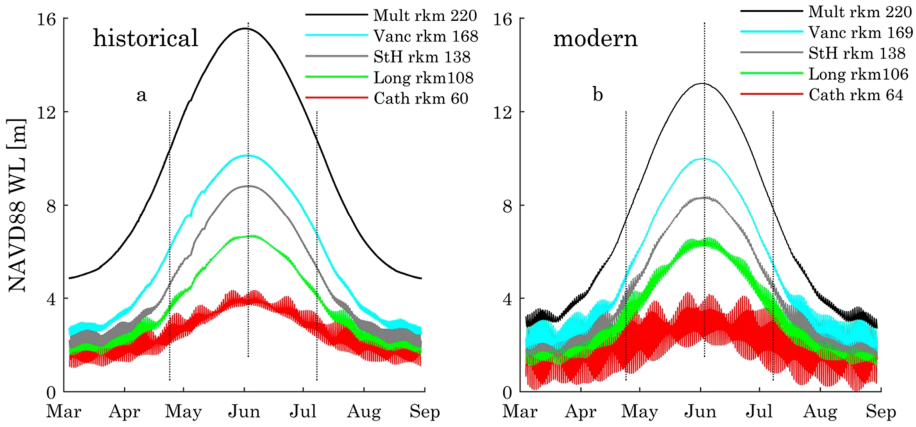

Figure 10. Peak water levels from the 6-month normal distribution flood in the (a) historical model and (b) modern models (Mult. = Multnomah Falls; Vanc = Vancouver; StH = St. Helens; Long = Longview; Cath = Cathlamet). Water levels measured relative to the North American Vertical Datum of 1988 (NAVD88).

construction, the lhs term $\frac{dh}{dQ}$ must necessarily increase (i.e., the slope in the rating curve must increase), unless changes in sectionally averaged velocity (first and second terms on rhs) outweigh changes in width (third term on rhs). The flow velocity is governed by the momentum equation, and further analysis is required to assess which terms dominate.

Thus, we estimate terms in the St. Venant equations in finite difference form with model outputs. Spatial derivatives are estimated using a Δx of 5 km, and a Δt of 10 min. The Columbia River Datum (Hickson, 1912) is used to approximate the average historical bed slope (S_0). The slope of the water level between two adjacent observation points minus the estimated bed slope approximates the water level gradient with respect to the bed slope ($\Delta h/\Delta x$).

$$\frac{1}{g}\frac{\Delta u}{\Delta t}+\frac{u}{g}\frac{\Delta u}{\Delta x}+\frac{\Delta h}{\Delta x}=S_0-S_f \tag{7}$$

An analysis of the output from the simulations show that the first acceleration term $\left(\frac{1}{g}\frac{\Delta u}{\Delta t}\right)$ in equation (7) is always negligible (see supporting information). The second acceleration term $\left(\frac{u}{g}\frac{\Delta u}{\Delta x}\right)$ is only significant near Beaver (rkm 87, see Figure 1) during the peak of the flood (see supporting information), and the momentum balance is usually between the pressure gradient ($\Delta h/\Delta x$) and the difference of the bed slope and the friction slope ($S_0 - S_f$). If the acceleration terms are negligible compared to the other remaining terms (as here), the St. Venant equation reduces to the diffusive wave approximation.

$$\frac{\Delta h}{\Delta x}=S_0-S_f \tag{8}$$

Figure 11 shows tidally averaged (~24.84 hr, 24 hr 50 min) water levels (first row), depth-averaged channel velocity (second row), water level gradient ($\Delta h/\Delta x$; third row), and bed stress (fourth row) during rising water levels (1), peak water levels (2), and falling water levels (3).

Results suggest that modern flows within the shipping channel have higher velocities than historical flows (Figures 11d–11f, second row). During all three phases of the flood, the velocity peaks at rkm 88, near Beaver (rkm 85). This is a relatively narrow section of the river and much of the historical floodplain in this area is now isolated by levees (see supporting information). Since the cross-section discharge is the same in both models, the lower channel velocity in the historical model means that the cross-sectional area must be larger. This is accomplished by floodplain inundation, which conveys some flow. This flow is relatively small, due to the high friction in the historical floodplain (modern currents would be larger, due to their larger Chezy coefficient).

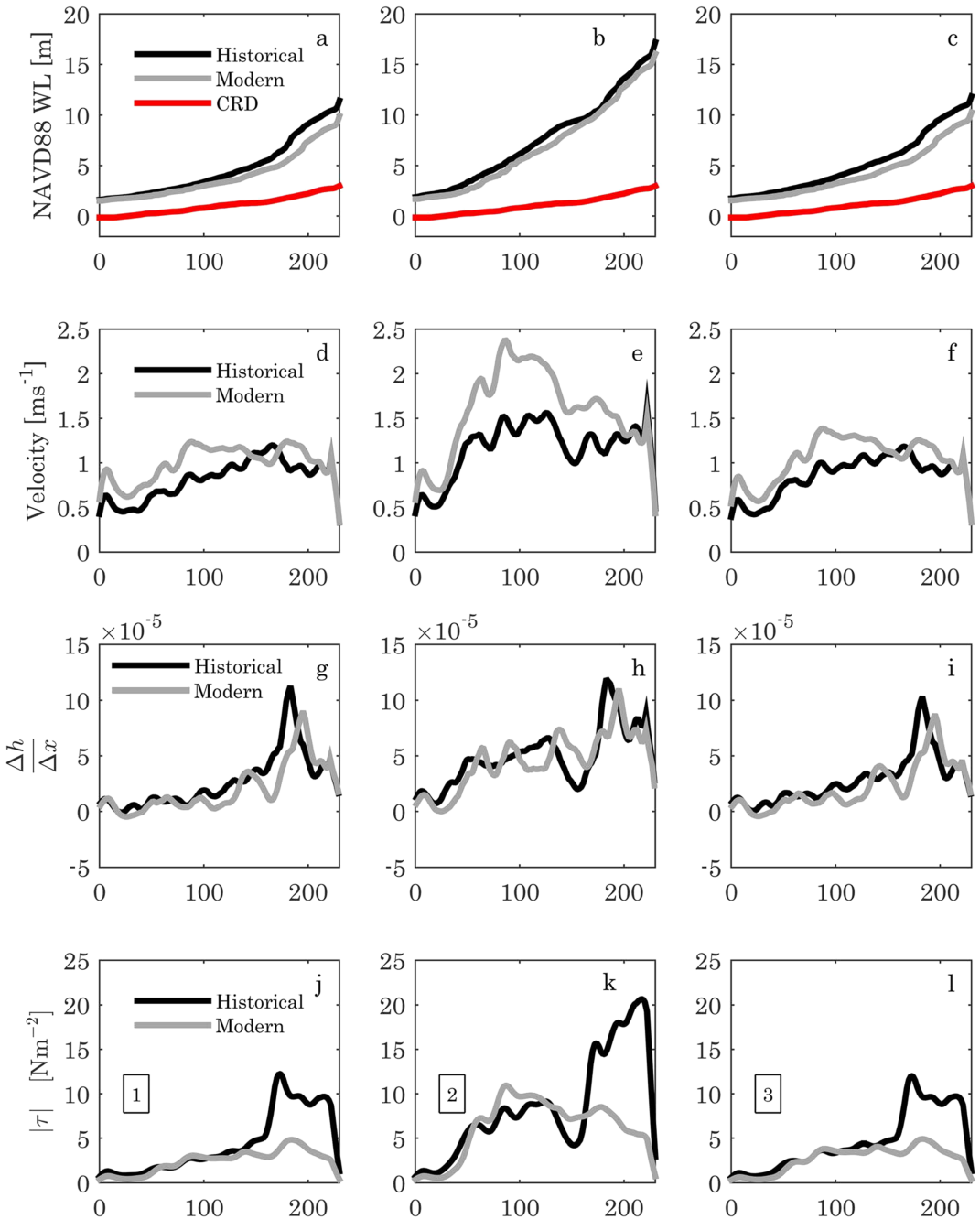

Figure 11. Tidally and depth averaged water level (row 1), channel velocity (row 2), water level gradient (row 3), and bed stress (row 4), in the historical and modern model during three phases of the 25×10^3-m^3/s flood simulation. 1 = rising limb; 2 = peak; 3 = falling limb. CRD = Columbia River Datum; NAVD88 = North American Vertical Datum of 1988.

Though the total water level drop between Portland and the ocean is similar in both models for the 25×10^3 m^3/s case, the spatial variability in the slope is different. In the historical model, during the peak of the flood $\Delta h/\Delta x$ decreases downstream of the Willamette confluence, likely due to the inundation of Sauvie Island (Figure 7). In the modern model, the isolation of the floodplain by levees affects water level gradients. For example, three small peaks in water level gradient occur near rkm 65, rkm 91, and rkm 139. The small peak at rkm 65 is likely caused by the isolation of the floodplain between Skamokawa and Wauna (see Figure 1 for place-name locations). The second smaller peak at rkm 91 is likely related to the isolation of the large floodplain near Beaver, (see Figure 1 and supporting information). The third smaller peak is likely related to

channel convergence upstream of St. Helens (rkm 139) and isolation of the floodplain on the east bank of the Columbia River upstream of rkm 139 (see Figure 3 and supporting information). To summarize, the differences in water level gradients between the modern and historical models are related to changes in friction, channel depth, and floodplain inundation, mostly driven by the presence of flood control levees present in the modern model.

Higher velocity in the modern model (Figures 11d–11f, second row) during flood conditions works to increase bed stress, compared to the historical condition; by contrast, smaller roughness in the modern model tends to decrease bed stress (see equation (3)). Our results suggest that during a 25×10^3-m^3/s flood, increased velocity and decreased roughness nearly compensate each other, producing similar water levels and surface gradients in both models. Hence, results show that during the rising and falling limbs of the flood modern and historical bed stress are nearly identical downstream of rkm 140 (Figures 11j and 11l, bottom row, first and third panels). During the peak flood, modern bed stress is slightly larger. Since the surface slope scales with τ/gh (Hoitink & Jay, 2016), the larger modern depth compensates for the larger bed stress, producing the previously mentioned similarities in average slope.

Spatial variability in bed stress also occurs between the modern and historical models, reflecting flow confinement. In the modern model, during the peak of the flood there is a large peak in bed stress at rkm 86 near Beaver (Figure 1), exceeding the historical bed stress (Figure 11k bottom row, middle panel). This peak in bed stress corresponds to the peak in depth averaged channel velocity (Figure 11e, second row, middle panel). Conversely, there is a large dip in historical bed stress at rkm 154 upstream of St. Helens, OR (Figure 1), where the Columbia River flows past Sauvie Island (Figure 11k, bottom row, middle panel). At this location, during the peak of the flood, there are also dips in the water level gradient and depth-averaged channel velocity (Figures 11e and 11h, second and third rows, middle panels). It appears that the inundation of Sauvie Island in the historical model diffused the flood wave and lowered the channel velocity and bed stress.

5. Conclusions

Numerical simulations of hydrodynamics on nineteenth-century and modern bathymetry, as well as analysis of water levels records, are used to investigate the evolution of tidal and flood processes in the LCRE. Channel deepening and reduced hydraulic roughness have caused MWLs to drop during low flow conditions, particularly upstream in the Portland/Vancouver metro area (0.5–1 m less, depending on river flow; Figure 6). Hence, though peak annual water levels in Portland have dropped primarily due to decreased river flow (Figure 5), navigation improvements, and diking play a significant role. At the same time that MWLs have dropped, tide amplitudes have increased, with the largest increase in M_2 during low flow conditions observed upstream of Astoria, at rkm 61 (Figure 4). These results are explainable as the effect of increased depth and reduced roughness, which decreases the damping of long waves (see, e.g., Friedrichs & Aubrey, 1994). These same factors reduce the surface slope during low flow (e.g., Jay et al., 2010; Ralston et al., 2019).

The reduced MWLs observed during low and moderate flow largely vanish during a high flow event, at least in the Portland/Vancouver area (~0.1-m difference). This occurs due to the increased channel velocity during modern, confined conditions, which acts to increase bed stress and surface slope. By contrast, historical flows overtopped the natural levees during large floods, reducing the channel velocity and providing large storage areas, both of which act to reduce the difference between historical and modern water levels, particularly in regions in which large floodplains exist (such as near Portland/Vancouver). At a larger discharge of 30×10^3 m^3/s, modern water levels would be ~0.5 m higher than historically in Portland/Vancouver, due to flow confinement. Once significant overbank flooding occurs in the modern model (around 35×10^3 m^3/s), historical and modern water levels are again similar. While such flow levels have not occurred since 1894, the combination of sea level rise and predictions of increased precipitation and runoff due to climate change (Najafi & Moradkhani, 2015) suggest that careful reassessment of system vulnerabilities is warranted.

Acknowledgments
Model output can be found at https://doi.org/10.15760/cee-data.01 on the PDXScholar repository. The Lower Columbia River Estuary Partnership is acknowledged for sharing the 2010 Lower Columbia Digital Terrain Model (https://www.estuarypartnership.org/). Water level data from gauges in the Columbia River downloaded from National Ocean and Atmospheric Administration website (https://tidesandcurrents.noaa.gov/). Water level data for the Portland (Morrison Bridge) and discharge data for the Columbia River at The Dalles are downloaded from the United States Geological Survey website (https://waterdata.usgs.gov/nwis/). Discharge data for the Columbia River at Bonneville are downloaded from Fish Passage Center website (http://www.fpc.org/river/flowspill/FlowSpill.asp). Digitized Portland water level data obtained from (and available) from the City of Portland, 1880–1964. U.S. Coastal Relief Model—Northwest Pacific downloaded from the National Geophysical Data Center Website (https://www.ngdc.noaa.gov/mgg/coastal/crm.html). Historical Lower Columbia River Estuary bathymetry data downloaded from University of Washington Wetland Ecosystem Team website (http://depts.washington.edu/wet/data.html). Funding was provided by the Office of Naval Research (award N00014-13-1-0084), the U.S. Army Corps of Engineers (award W1927N-14-2-0015), the National Science Foundation (award 1455350), and internal Portland State funding. I would like to especially acknowledge the work of my co-author, the late Drew Mahedy, for his assistance in the development of the hydrodynamic models, and recovery of nineteenth-century tidal data.

References

Act to Improve Rivers and Harbors, 20 Stat. 152 (1878)
Arcement Jr, G. J., & Schneider, V. R. (1989). Guide for selecting Manning's roughness coefficients for natural channel and floodplains. United States Geological Survey Water Supply Paper 2339, *pubs.usgs.gov/wsp/2339/report.pdf*
Avi, B. (2017). Statewide levee database for Oregon, Release 1.0: Major agricultural and urban areas in Western Oregon and along the Columbia River, report, Oregon Department of Geology and Mineral Industries, Portland, OR.

Bottom, D. L., Simenstad, C. A., Burke, J., Baptista, A. M., Jay, D. A., Jone, K. K., et al. (2005). Salmon at River's End: The role of the estuary in the decline and recovery of Columbia River salmon, Technical Memorandum NMDS-NWFSC-68. Seattle, WA: NOAA.
Burgette, R. J., Weldon, R. J., & Schmidt, D. A. (2009). Interseismic uplift rates for western Oregon and along-strike variation in locking on the Cascadia subduction zone. *Journal of Geophysical Research*, *114*, B01408. https://doi.org/10.1029/2008JB005679
Burke, J. L. (2010). Georeferenced historical topographic survey maps of the Columbia River Estuary, School of Aquatic and Fishery Sciences, University of Washington, Seattle, WA. Funded by the U.S. Corps of Engineers, Portland District and NOAA Northwest Fisheries.
Cox, R., Wadsworth, R. A., & Thomson, A. G. (2003). Long-term changes in salt marsh extent affected by channel deepening in a modified estuary. *Continental Shelf Research*, *23*(17-19), 1833–1846. https://doi.org/10.1016/j.csr.2003.08.002
Cunge, J. A., Holly, F. M., & Verwey, A. (1980). *Practical aspects of computational river hydraulics* (p. 420). London: Pitman.
Dodge, R. O. (1976). Construction of the 40-foot channel in Columbia River.
Egbert, G. D., & Erofeeva, S. Y. (2002). Efficient inverse modeling of barotropic ocean tides. *Journal of Atmospheric and Oceanic Technology*, *19*(2), 183–204. https://doi.org/10.1175/1520-0426(2002)019<0183:EIMOBO>2.0.CO;2
Elias, E. P., Gelfenbaum, G., & Van der Westhuysen, A. J. (2012). Validation of a coupled wave-flow model in a high-energy setting: The mouth of the Columbia River. *Journal of Geophysical Research*, *117*, C09011. https://doi.org/10.1029/2012JC008105
Familkhalili, R., & Talke, S. A. (2016). The effect of channel deepening on tides and storm surge: A case study of Wilmington, NC. *Geophysical Research Letters*, *43*, 9138–9147. https://doi.org/10.1002/2016GL069494
Friedrichs, C. T., & Aubrey, D. G. (1994). Tidal propagation in strongly convergent channels. *Journal of Geophysical Research*, *99*(C2), 3321–3336. https://doi.org/10.1029/93JC03219
Giese, B. S., & Jay, D. A. (1989). Modelling tidal energetics of the Columbia River Estuary. *Estuarine, Coastal and Shelf Science*, *29*(6), 549–571. https://doi.org/10.1016/0272-7714(89)90010-3
Hamilton, P. (1990). Modeling salinity and circulation for Columbia River Estuary. *Progress in Oceanography*, *25*(1-4), 113–156. https://doi.org/10.1016/0079-6611(90)90005-M
Helaire, L.T. (2016). Modeling of historic Columbia River flood impacts based on Delft3D simulations.
Henshaw, F. F., & Dean, H. J. (1915). Surface water supply of Oregon. US Government Printing Office.
Hickson, R. E. (1912). A report on the establishment of river gages on lower Columbia & Willamette rivers. Report to the US Army Corps of Engineers.
Hickson, R. E. (1961). Columbia River ship channel improvement and maintenance. *Journal of the Waterways and Harbors Division*, *87*(3), 71–94.
Hickson, R. E., & Rodolf, F. W. (1950). History of Columbia River jetties. *Coastal Engineering Proceedings*, *1*(1), 32.
Hoitink, A. J. F., & Jay, D. A. (2016). Tidal river dynamics: Implications for deltas. *Reviews of Geophysics*, *54*, 240–272. https://doi.org/10.1002/2015RG000507
Hydraulics, D. (2006). Delft3D-FLOW user manual. Delft, the Netherlands.
Jay, D. A. (2009). Evolution of tidal amplitudes in the eastern Pacific Ocean. *Geophysical Research Letters*, *36*, L04603. https://doi.org/10.1029/2008GL036185
Jay, D. A., Borde, A. B., & Diefenderfer, H. L. (2016). Tidal-fluvial and estuarine processes in the Lower Columbia River: II. Water level models, floodplain wetland inundation, and system zones. *Estuaries and Coasts*, *39*(5), 1299–1324. https://doi.org/10.1007/s12237-016-0082-4
Jay, D. A., Leffler, K., & Degens, S. (2010). Long-term evolution of Columbia River tides. *Journal of Waterway, Port, Coastal, and Ocean Engineering*, *137*(4), 182–191.
Kärnä, T., & Baptista, A. M. (2016). Evaluation of a long-term hindcast simulation for the Columbia River estuary. *Ocean Modelling*, *99*, 1–14. https://doi.org/10.1016/j.ocemod.2015.12.007
Kärnä, T., Baptista, A. M., Lopez, J. E., Turner, P. J., McNeil, C., & Sanford, T. B. (2015). Numerical modeling of circulation in high-energy estuaries: A Columbia River estuary benchmark. *Ocean Modelling*, *88*, 54–71. https://doi.org/10.1016/j.ocemod.2015.01.001
Kassenbaum, C. (2011). Structure and hydraulic analysis of Columbia River pile dikes, 192 pp., AECOM, Seattle, WA xx.
Keshtpoor, M., Puleo, J. A., Shi, F., & Ma, G. (2015). 3D numerical simulation of turbulence and sediment transport within a tidal inlet. *Coastal Engineering*, *96*, 13–26. https://doi.org/10.1016/j.coastaleng.2014.10.009
Kidby, H. A., & Oliver, J. G. (1965). Erosion and accretion along Clatsop Spit. In Proceedings Santa Barbara specialty conference. ASCE.
Leffler, K. E., & Jay, D. A. (2009). Enhancing tidal harmonic analysis: Robust (hybrid L1/L2) solutions. *Continental Shelf Research*, *29*(1), 78–88. https://doi.org/10.1016/j.csr.2008.04.011
Lockett, J. B. (1959). Interim consideration of the Columbia River entrance. *Journal of the Hydraulics Division*, *85*(1), 17–40.
Manning, A. J., Van Kessel, T., Melotte, J., Sas, M., Winterwerp, H., & Pidduck, E. L. (2011). On the consequence of a new tidal dock on the sedimentation regime in the Antwerpen area of the Lower Sea Scheldt. *Continental Shelf Research*, *31*(10), S150–S164. https://doi.org/10.1016/j.csr.2010.10.008
Marcoe, K., & Pilson, S. (2017). Habitat change in the lower Columbia River estuary, 1870–2009. *Journal of Coastal Conservation*, *21*(4), 505–525. https://doi.org/10.1007/s11852-017-0523-7
Martins, F., Leitão, P., Silva, A., & Neves, R. (2001). 3D modelling in the Sado estuary using a new generic vertical discretization approach. *Oceanologica Acta*, *24*, 51–62. https://doi.org/10.1016/S0399-1784(01)00092-5
McIndoe, J. F., & Thomson, E. B. (1911). Willamette River, Oregon, from Portland to Oregon City (in three sheets), map, U.S. Army Corp of Engineers, Washington DC xx.
Mote, P. W., & Salathé, E. P. (2010). Future climate in the Pacific Northwest. *Climatic Change*, *102*(1-2), 29–50. https://doi.org/10.1007/s10584-010-9848-z
Munoz, S. E., Giosan, L., Therrell, M. D., Remo, J. W., Shen, Z., Sullivan, R. M., et al. (2018). Climatic control of Mississippi River flood hazard amplified by river engineering. *Nature*, *556*(7699), 95–98. https://doi.org/10.1038/nature26145
Naik, P. K., & Jay, D. A. (2005). Estimation of Columbia River virgin flow: 1879 to 1928. *Hydrological Processes: An International Journal*, *19*(9), 1807–1824. https://doi.org/10.1002/hyp.5636
Naik, P. K., & Jay, D. A. (2011). Distinguishing human and climate influences on the Columbia River: Changes in mean flow and sediment transport. *Journal of Hydrology*, *404*(3-4), 259–277. https://doi.org/10.1016/j.jhydrol.2011.04.035
Najafi, M. R., & Moradkhani, H. (2015). Multi-model ensemble analysis of runoff extremes for climate change impact assessments. *Journal of Hydrology*, *525*, 352–361. https://doi.org/10.1016/j.jhydrol.2015.03.045
National Geophysical Data Center (2003). U.S. Coastal Relief Model—Northwest Pacific. National Geophysical Data Center, NOAA. https://doi.org/10.7289/V5H12ZXJ

Nicolle, A., & Karpytchev, M. (2007). Evidence for spatially variable friction from tidal amplification and asymmetry in the Pertuis Breton (France). *Continental Shelf Research*, *27*(18), 2346–2356. https://doi.org/10.1016/j.csr.2007.06.005

Orem, H. M. (1968). Discharge in the lower Columbia River basin, 1928-65 (Vol. 550). US Geological Survey.

Passeri, D. L., Hagen, S. C., Medeiros, S. C., & Bilskie, M. V. (2015). Impacts of historic morphology and sea level rise on tidal hydrodynamics in a microtidal estuary (Grand Bay, Mississippi). *Continental Shelf Research*, *111*, 150–158. https://doi.org/10.1016/j.csr.2015.08.001

Pawlowicz, R., Beardsley, B., & Lentz, S. (2002). Classical tidal harmonic analysis including error estimates in MATLAB using T_TIDE. *Computers & Geosciences*, *28*(8), 929–937. https://doi.org/10.1016/S0098-3004(02)00013-4

Pinter, N., Jemberie, A. A., Remo, J. W., Heine, R. A., & Ickes, B. S. (2008). Flood trends and river engineering on the Mississippi River system. *Geophysical Research Letters*, *35*, L23404. https://doi.org/10.1029/2008GL035987

Public Acts of the 47th Congress, 1882, Session I, Ch. 375 (1882)

Ralston, D. K., Talke, S., Geyer, W. R., Al-Zubaidi, H. A., & Sommerfield, C. K. (2019). Bigger tides, less flooding: Effects of dredging on barotropic dynamics in a highly modified estuary. *Journal of Geophysical Research: Oceans*, *124*, 196–211. https://doi.org/10.1029/2018JC014313

River and Harbor Act of 1905, Pub. L. No. 58-215, 33 Stat. 1117 (1905)

River and Harbor Act of 1912, 37 Stat. 201 (1912)

River and Harbor Act of 1930, Pub. L. No. 71-520, 46 Stat. 918 (1930)

River and Harbor Act of 1954, Pub. L. No 83-780, 68 Stat. 1248 (1954)

Rivers and Harbors Act of 1962, Pub. L. No 87-874, 76 Stat. 1173 (1962)

Rivers and Harbors Appropriation Act of 1899, 30 Stat. 1121 (1899)

Roelvink, J. A., & Van Banning, G. K. F. M. (1995). Design and development of DELFT3D and application to coastal morphodynamics. *Oceanographic Literature Review*, *11*(42), 925.

Salathé, E. P. Jr., Hamlet, A. F., Mass, C. F., Lee, S. Y., Stumbaugh, M., & Steed, R. (2014). Estimates of twenty-first-century flood risk in the Pacific Northwest based on regional climate model simulations. *Journal of Hydrometeorology*, *15*(5), 1881–1899. https://doi.org/10.1175/JHM-D-13-0137.1

Sandbach, S. D., Nicholas, A. P., Ashworth, P. J., Best, J. L., Keevil, C. E., Parsons, D. R., et al. (2018). Hydrodynamic modelling of tidal-fluvial flows in a large river estuary. *Estuarine, Coastal and Shelf Science*, *212*, 176–188. https://doi.org/10.1016/j.ecss.2018.06.023

Sherwood, C. R., Jay, D. A., Harvey, R. B., Hamilton, P., & Simenstad, C. A. (1990). Historical changes in the Columbia River estuary. *Progress in Oceanography*, *25*(1-4), 299–352. https://doi.org/10.1016/0079-6611(90)90011-P

Sleigh, P. A., Gaskell, P. H., Berzins, M., & Wright, N. G. (1998). An unstructured finite-volume algorithm for predicting flow in rivers and estuaries. *Computers & Fluids*, *27*(4), 479–508. https://doi.org/10.1016/S0045-7930(97)00071-6

Talke, S. A., & Jay, D. A. (2013). Nineteenth century North American and Pacific tidal data: Lost or just forgotten? *Journal of Coastal Research*, *29*(6a), 118–127. https://doi.org/10.2112/JCOASTRES-D-12-00181.1

Talke, S. A., & Jay, D. A. (2017). Archival water-level measurements: Recovering historical data to help design for the future.

Tanaka, S., Bunya, S., Westerink, J. J., Dawson, C., & Luettich, R. A. (2011). Scalability of an unstructured grid continuous Galerkin based hurricane storm surge model. *Journal of Scientific Computing*, *46*(3), 329–358. https://doi.org/10.1007/s10915-010-9402-1

Templeton, W. J., & Jay, D. A. (2012). Lower Columbia River sand supply and removal: Estimates of two sand budget components. *Journal of Waterway, Port, Coastal, and Ocean Engineering*, *139*(5), 383–392.

Thorn, F. M. (1888). Columbia River Sheet No. 6 Fales Landing to Portland, United States Coast and Geodetic Survey, Washington, D.C.

United States Weather Bureau (1878-1888). Discharge estimates of the Willamette River in Salem, OR, National Weather Service Archives, Portland, OR.

United States Weather Bureau (1879-1898). Water level records from the Willamette River in Portland, OR, City of Portland Archives, Portland, OR.

United States Weather Bureau (1893-1946). Daily river stages at river gage stations on the principals rivers of the United States, 1893-1946.

USACE (1915). Report of the Secretary of War, Annual Report of the Chief of Engineers for historical summary giving the scope of previous projects for the improvement of certain rivers and harbors, U.S. Govt. Print. Off., Washington, D.C.

USACE (1963). Water Surface Profiles, Floods—1876, 1894, 1933, 1946, 1948, 1950 and 1956, U.S. Army Corp of Engineers, Portland District.

USACE (1997). February 1996 post flood report: Hydrometeorological evaluation, USACE, Portland, OR.

USACE (2010). Lower Columbia River Digital Terrain Model, USACE, Portland, OR.

USACE (n.d.). Building Strong® at the Mouth of the Columbia River. Retrieved from https://www.nwp.usace.army.mil/Locations/Oregon-Coast/Mouth-of-the-Columbia/

USC&GS (1877). United States National Coast & Geodetic Survey Columbia River tide logs, National Archives, College Park, MD.

Waananen, A. O., Harris, D. D., & Williams, R. C. (1970). Floods of December 1964 and January 1965 in the Far Western States: Part 2. Streamflow and sediment data. US Government Printing Office.

Wang, J., Yi, S., Li, M., Wang, L., & Song, C. (2018). Effects of sea level rise, land subsidence, bathymetric change and typhoon tracks on storm flooding in the coastal areas of Shanghai. *Science of the Total Environment*, *621*, 228–234. https://doi.org/10.1016/j.scitotenv.2017.11.224

Wang, Z. B., Tse, M. L., & Lau, S. C. (2012). A study on sedimentation of tidal rivers and channels flowing into deep bay with a Delft3D model. In *Asian And Pacific Coasts 2011* (pp. 1444–1451). Hong Kong.

Water Resources Development Act of 1999, Pub. L. 106-53, 113 Stat. 269 (1999)

Zaron, E. D., & Jay, D. A. (2014). An analysis of secular change in tides at open-ocean sites in the Pacific. *Journal of Physical Oceanography*, *44*(7), 1704–1726. https://doi.org/10.1175/JPO-D-13-0266.1

Zhang, Y., & Baptista, A. M. (2008). SELFE: A semi-implicit Eulerian–Lagrangian finite-element model for cross-scale ocean circulation. *Ocean modelling*, *21*(3-4), 71–96. https://doi.org/10.1016/j.ocemod.2007.11.005

Zhang, Y., Baptista, A. M., & Myers, E. P. (2004). A cross-scale model for 3D baroclinic circulation in estuary–plume–shelf systems: I. Formulation and skill assessment. *Continental Shelf Research*, *24*(18), 2187–2214. https://doi.org/10.1016/j.csr.2004.07.021